CHEMISTRY & SUSTAINABILITY

CHEMSUSCHEM

ENERGY & MATERIALS

Accepted Article

Title: Single-site ruthenium pincer complex knitted in porous organic polymers for green dehydrogenation of formic acid in aqueous medium

Authors: Kuo-Wei Huang, Xinbo Wang, Eleanor Ang, Chao Guan, Qinggang Zhang, Wenting Wu, Pengxin Liu, Nanfeng Zheng, Daliang Zhang, Sergei Lopatin, and Zhiping Lai

This manuscript has been accepted after peer review and appears as an Accepted Article online prior to editing, proofing, and formal publication of the final Version of Record (VoR). This work is currently citable by using the Digital Object Identifier (DOI) given below. The VoR will be published online in Early View as soon as possible and may be different to this Accepted Article as a result of editing. Readers should obtain the VoR from the journal website shown below when it is published to ensure accuracy of information. The authors are responsible for the content of this Accepted Article.

To be cited as: *ChemSusChem* 10.1002/cssc.201801980

Link to VoR: http://dx.doi.org/10.1002/cssc.201801980

A Journal of ChemPubSoc Europe

WILEY-VCH

www.chemsuschem.org

DOI: 10.1002/((please add manuscript number))
Article type: Communication

Single-site ruthenium pincer complex knitted in porous organic polymers for green dehydrogenation of formic acid in aqueous medium

Xinbo Wang [a,À], Eleanor Ang Pei Ling [a,À], Chao Guan [a], Qinggang Zhang [b], Wenting Wu [b], Pengxin Liu [c], Nanfeng Zheng [c], Daliang Zhang [d], Sergei Lopatin [d], Zhiping Lai [a*] and Kuo-Wei Huang [a*]

[a.] Division of Physical Science and Engineering, King Abdullah University of Science and Technology (KAUST), Thuwal, 23955-6900, Kingdom of Saudi Arabia.
[b.] State Key Laboratory of Heavy Oil Processing, College of Chemical Engineering, China University of Petroleum (East China), Qingdao 266580, China.
[c.] State Key Laboratory of Physical Chemistry of Solid Surfaces, iChEM, Department of Chemistry, College of Chemistry and Chemical Engineering, Xiamen University, Xiamen 361005, China.
[d.] King Abdullah University of Science and Technology (KAUST), Core Labs, Thuwal, 23955-6900, Saudi Arabia
[À] These authors contributed equally to this work.
[*] Corresponding authors. Email: hkw@kaust.edu.sa (K.-W.H.), zhiping.lai@kaust.edu.sa (Z. L.)

Abstract:

Owing to its capacity for reversible hydrogen storage, formic acid (FA) holds great promise as an energy carrier alternative to conventional fossil fuels systems. While the decomposition of FA to hydrogen (H_2) and carbon dioxide (CO_2) through homogeneous catalysis has been well-established, the selective and efficient dehydrogenation of FA by a robust heterogeneous catalyst remains a challenge. Herein, a novel heterogeneous ruthenium-pincer framework with single-atomic sites was prepared in one step by the direct knitting of a phosphorous-nitrogen PN^3P-pincer ruthenium complex in a porous organic polymer. The heterogeneous ruthenium complex efficiently dehydrogenates formic acid in both organic and aqueous media with remarkably enhanced stability. Notably, no detectible CO was generated and a turnover number of 145,300 was attained in a continuous experiment with no significant decline in catalytic reactivity (in sharp contrast, total TON of only 5,600 was obtained with the homogeneous analog under the same conditions). The single-atomic sites in the porous framework allowed the combination of the desirable attributes of high reactivity and selectivity of a homogeneous catalyst with the significantly enhanced catalyst stability and reusability benefits of heterogeneous catalysis.

Keywords: Single-site, Pincer, Porous organic polymers, Heterogeneous catalysis, Formic acid dehydrogenation.

With the rapid consumption of fossil fuels to meet the ever increasing global energy demand,[1] one of the key challenges of this century is to identify a sustainable supply of carbon-neutral energy and the corresponding carrier systems.[2] In this regard, hydrogen has generated considerable interest as an environment-friendly efficient energy carrier[3] because it can be used in fuel cells to generate electricity with water as the only by-product. However, the

This article is protected by copyright. All rights reserved.

widespread application of hydrogen energy technologies has not been realized as yet, primarily because of inherent issues related to hydrogen being a gas under ambient conditions, which limit its volumetric energy density and present difficulties in liquefaction and storage.[4] Hence, extensive investigations of hydrogen-rich liquids have been conducted for on-demand hydrogen release. Formic acid (FA) is a promising hydrogen energy carrier[5] owing to its high volumetric capacity (53 g $L^{ï 1}$ or 1.77 kWh $L^{ï 1}$), low toxicity, and portability. In addition, FA can readily release hydrogen through catalytic dehydrogenation with CO_2 as a by-product and can be potentially regenerated by the catalytic hydrogenation of CO_2 to offer a sustainable energy storage system.[6]

While developing direct FA fuel cells (DFACs) is still challenging because of catalyst poisoning,[5, 7] hydrogen generation from formic acid appears to be a great alternative as hydrogen fuel cells are considered as a relatively mature technology and have been commercialized in fuel cell-based vehicles. Over the last decades, many important contributions have been made to this area and various homogeneous[8] and heterogeneous[9] catalysts were established. Typically, homogeneous catalytic systems, especially those based on transition metal-organic complexes (e.g. pincer complexes), exhibit very high activity and selectivity. Unfortunately, they also have relatively low stability and recyclability, resulting in a high overall application cost. In contrast, heterogeneous catalysts reduce these costs because of their higher durability, albeit their low activity and generation of CO impurity prohibit their widespread applications. New materials that combine the advantages of both homogeneous and heterogeneous catalysis will undoubtedly benefit the development of hydrogen from formic acid for practical applications.

In our previous work, we developed a ^{t}Bu-PN^{3}P-pincer ruthenium complex bearing a dearomatized pyridine moiety with an imine arm that showed excellent catalytic performance in the FA dehydrogenation reaction, attaining a turnover number (TON) of 1,100,000 over 150 h and turnover frequency (TOF) of 7,300 $h^{ï 1}$ at 90 °C.[10] The tridentate organic part of the coordinated pincer enforced a meridional geometry on the metal center upon complexation, resulting in a unique balance of stability versus reactivity.[11] Mechanistic studies showed that the PN^{3}P ligand played an important role in the FA dehydrogenation reaction via the aromatizationï dearomatization process. This process was favorable to the dehydrogenation pathway and as a result, the dehydrogenation/dehydration selectivity was greatly improved.[10] The promising activity of the ^{t}Bu-PN^{3}P-Ru catalyst prompted us to employ a more economical ligand using phenyl to replace the *t*-butyl groups. While the resulting Ph-PN^{3}P-pincer ruthenium complex demonstrated high catalytic activity to selectively converted CO_2 captured from air and H_2 to formate,[12] only far-fetched durability of the catalyst was observed in the selective decomposition of FA to H_2 and CO_2. When the catalytic reaction was conducted in aqueous dimethyl sulfoxide (DMSO) at 90 °C, the initial high TOF value of 1,800 $h^{ï 1}$ decreased sharply and the total TON of only 5,600 was reached.

Immobilization of homogeneous catalysts[13] by covalently attaching the ligand to a solid porous support can enhance their stability and recyclability.[14] For example, the pincer complex systems immobilized on metal-organic frameworks (MOFs) developed by Wade et al. and Farha et al. exhibit greatly improved stability.[15] However, anchoring a pincer complex on a heterogeneous substrate to obtain a single-site dispersed catalyst is quite challenging and tedious.[15b] To date, there exist only a limited number of pincer-containing heterogeneous catalysts and they all require special design and multi-step syntheses. Therefore, a direct method

This article is protected by copyright. All rights reserved.

for incorporating existing pincer complexes into a porous heterogeneous framework with single-site dispersion would be undoubtedly important and useful.

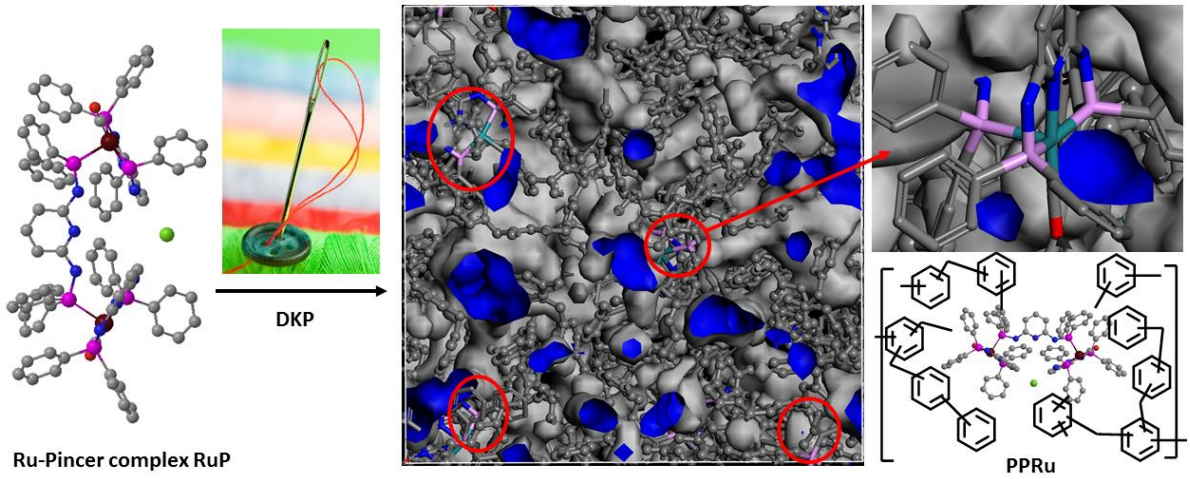

Scheme 1. Schematic illustration for preparation of PPRu by direct knitting of the Ph-PN^{3}P-pincer ruthenium complex RuP into porous organic polymer. Conditions for the direct knitting polymerization (DKP): RuP (0.1 mmol), Benzene (4 mmol), 1,2-dichloroethane (40 ml), FeCl3 (12 mmol), 80 °C for 24 h.

In this context, porous organic polymers (POPs)[16] have attracted a lot of attention as a new class of porous materials because of their unique properties, which include a large surface area, ease of preparation, and low cost. Moreover, the robust covalent bonds used to construct the POPs bestow high chemical and thermal stability. These features make POPs a promising platform for heterogeneous catalysis.[17] Herein, we report the one-step synthesis of a novel heterogeneous ruthenium compound (**PPRu**) with single-atomic sites via direct knitting of the Ph-PN^{3}P-pincer ruthenium complex (**RuP**) in a three-dimensional (3D) porous polymer network (Scheme 1). Structural and compositional analysis of the synthesized **PPRu** revealed that the ruthenium pincer units were successfully incorporated into the porous polymer network. The single-atomic Ru sites in **PPRu** were confirmed and characterized by high-angle annular dark-field scanning transmission electron microscopy (HAADF-STEM) and extended X-ray adsorption fine structure analysis (EXAFS). It was found that the heterogeneous ruthenium complex exhibited high catalytic performance and significantly enhanced stability towards FA dehydrogenation in both organic and aqueous media.

The Ph-PN^{3}P-pincer ruthenium complex (**RuP**) was prepared following the reported procedure by us.[12] Subsequently, the heterogeneous ruthenium compound **PPRu** was synthesized in one-step via hyper-crosslinking (Scheme 1).[14c, 18] In this method, dimethoxymethane was employed as an external crosslinker to combine the phenyl groups in **RuP** and simple aromatic compounds (benzene) with rigid methylene bridges via $FeCl_3$-catalyzed Friedelï Crafts reaction.[19] The Ru content loading was carefully controlled by adjusting the molar ratio of the pincer complex to the benzene monomer and the crosslinker to ensure sufficient space between the ruthenium pincer sites. Inductively coupled plasma optical emission spectroscopic (ICP-OES) analysis showed that the Ru content of **PPRu** was 1.58 wt% and elemental analysis (EA) showed that the N content was 1.08 wt%. The molar ratio of Ru to N was close to the theoretical value of 2:9, which implied that the structure of the PN^{3}P-pincer ruthenium complex was unchanged.

This article is protected by copyright. All rights reserved.

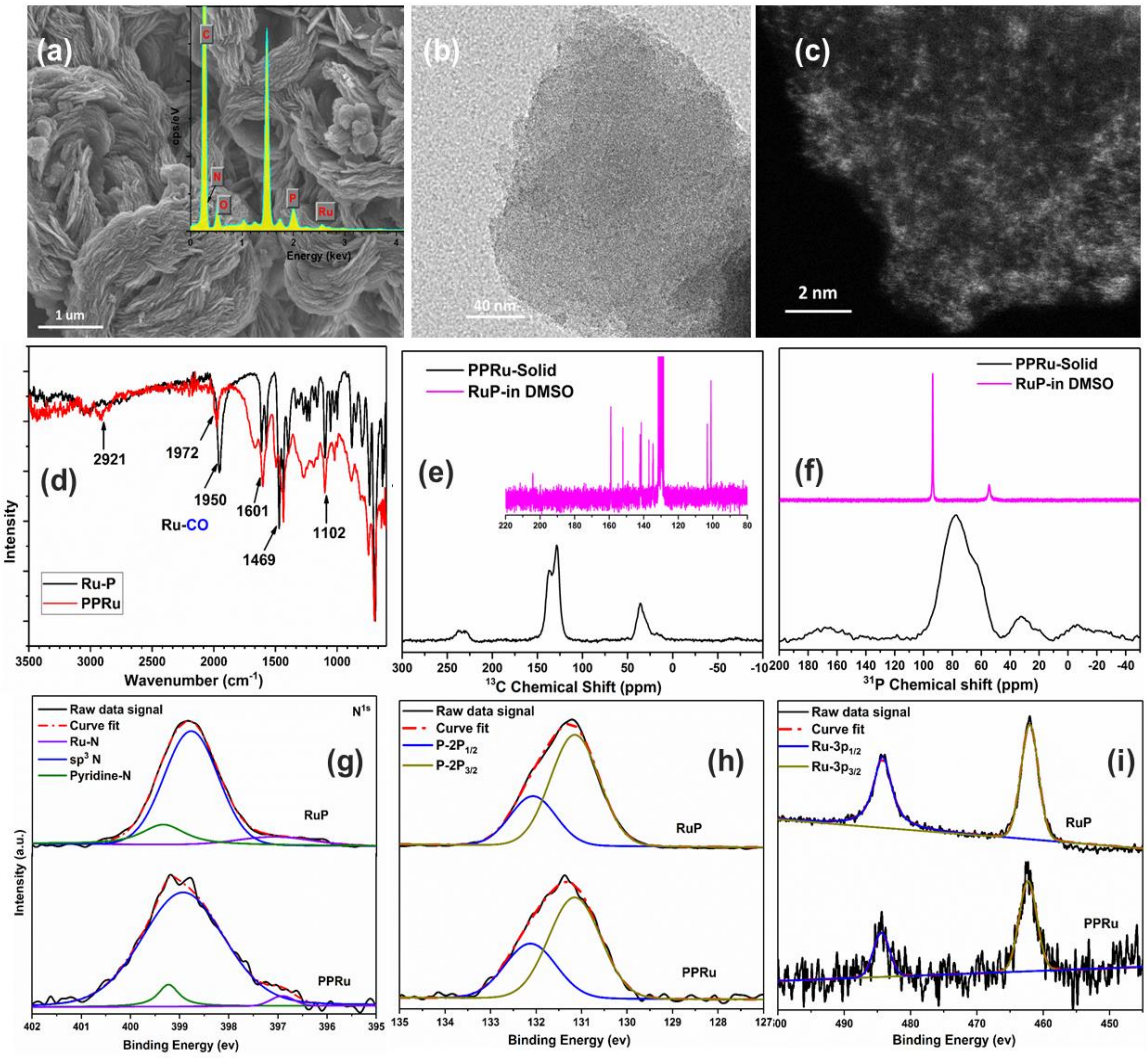

Figure 1. (a) SEM, (b) HRTEM, and (c) HAADF-STEM images of **PPRu**, inset in (a) is the extracted elemental spectrum; (d) FTIR, (e) ^{13}C NMR, (f) ^{31}P NMR, and (gï i) XPS spectra of Ru-pincer complex **RuP** and **PPRu**.

The surface morphology of **PPRu** was probed by SEM and TEM. The SEM image of **PPRu** shows the 3D architecture with interconnecting thin nanosheets (Figure 1a). The thin wrinkled morphology was clearly resolved by high resolution TEM (Figure 1b). Interestingly, in the high-resolution HAADF-STEM (atomic number or so-called Z-contrast) image, many uniformly distributed bright dots of sub-nm size were observed (Figure 1c). These small dots can be identified as single atoms of the heaviest element present, i.e. Ru. In addition, energy-dispersive X-ray spectroscopy (EDS) and elemental mapping analysis revealed a coherent existence of Ru, P, and N throughout the imaged area (Figure S1, Electronic Supplementary Information (ESIÀ)).

The successful growth of the hyper-crosslinked polymer network with incorporation of the ruthenium pincer units was confirmed by FTIR, solid-state ^{13}C-NMR, ^{31}P-NMR, and X-ray photoelectron spectroscopy (XPS). The pincer complex of **RuP**, whose structure has been previously confirmed by single-crystal X-ray diffraction,[12] was used for comparison. The FTIR spectrum of **PPRu** (Figure 1d) showed a peak at 1102 cm$^{\bar{1}\,1}$ corresponding to the Pï Ar

This article is protected by copyright. All rights reserved.

stretching vibrations. The peak at 1950 cm^{-1} of the ruthenium pincer complex was characteristic of the carbonyl group and shifted slightly to 1972 cm^{-1} in **PPRu**. The peaks located around 3100–3000, 1600–1450, 1250–950, and 900–650 cm^{-1} corresponded to the aromatic C–H stretching, aromatic ring skeleton stretching, and C–H out-of-plane and in-plane bending vibrations of the benzene ring, respectively.[14c] Moreover, the peak at 2921 cm^{-1} could be assigned to the alkyl C–H stretching vibrations. These observations indicated that the aromatic precursors were successfully connected via methylene linkers.[19] In the ^{13}C CP/MAS NMR spectrum of **PPRu** (Figure 1e), the carbon signals of the ruthenium pincer complex could not be identified because of its low loading in the polymer network as well as the low sensitivity of solid-state NMR. The characterization results matched those of the reported hyper-crosslinked polymer,[20] showing that a similar polymer network had formed. Specifically, the two resonance peaks near 137 and 128 ppm could be attributed to the substituted and non-substituted aromatic carbon, respectively, and the resonance peak near 37 ppm was assigned to the methylene linker carbon. Compared to the ^{31}P NMR peaks of RuP in DMSO-d_6 solution, those of solid **PPRu** were broader and shifted upfield by ~20 ppm (Figure 1f).

The surface composition and chemical state of **PPRu** were further analyzed by XPS. The XPS survey scan revealed the existence of C, N, P, and Ru elements (Figure S2). The high-resolution N 1s spectrum (Figure 2g) could be deconvoluted into three peaks centered at the binding energies of 399.3, 398.8, and 396.9 eV, which could be attributed to graphitic, non-coordinated pyridinic, and Ru-coordinated pyridinic N, respectively. The peak shift from 398.8 to 396.9 eV could be explained by interactions between the metal and pyridinic N, involving the transfer of electrons from ruthenium to pyridinic nitrogen. The P 2p spectrum (Figure 1h) showed two peaks, P $2p_{3/2}$ (131.2 eV) and P $2p_{1/2}$ (132.1 eV), which accounted for the effect of spin-orbit splitting at the 2p level with the expected separation of 0.9 eV [20] and only the presence of only one P-containing surface species. Compared to the P $2p_{3/2}$ binding energy of elemental phosphorus (130.2 eV), this binding energy was slightly higher, indicating that the P were coordinated to Ru and there was no oxidation of P to phosphate (binding energy of 133.2 eV) in the direct knitting process.[14c] In order to avoid interferences from the carbon substrates arising from the overlap of the C 1s and Ru 3d core-levels, Ru was analyzed by its 3p state instead of the typical 3d spectra.[21] The Ru 3p region (Figure 1i) reveals the presence of two doublet peaks for Ru $3p_{3/2}$ and Ru $3p_{1/2}$ centered at 461.8 and 484.2 eV, respectively, for the **RuP** species, and 462.3 eV and 484.4, respectively, for **PPRu**, implying that Ru was present in the +2 oxidation state in both samples.

The chemical state and coordination environment of the Ru atoms in **PPRu** were further investigated by EXAFS and X-ray absorption near-edge structure (XANES) spectroscopies. Expectedly, **PPRu** gave similar signals as the Ru-pincer precursor. The Fourier transform (FT) k^3-weighted $\chi(k)$ function of the EXAFS spectra as well as wavelet transformations (WT) are shown in Figure 2a–c, f and the assignment of the signals to Ru–C(N), Ru–O, Ru–Ru, or Ru–O–Ru interaction was based on EXAFS wavelet transform analysis of the reference materials. In contrast to the Ru foil and Ru oxide reference materials, **PPRu** did not present a prominent peak at the positions of either Ru–Ru or Ru–O coordination, supporting the conclusion that most of the Ru metal existed as mononuclear Ru centers in the **PPRu** sample. The WT intensity maximum detected at ~5.3 $Å^{-1}$ was well resolved as the main peak in the FT spectrum at 1.8 Å for the Ru-pincer **RuP** and **PPRu**, and corresponded to the horizontal axis Ru–P contribution. The small side peak at 1.1 Å in the FT spectrum, along with its weak intensity signal in WT, was attributed to the coordination of Ru–N/C. Accompanying the weaker intensity maximum

This article is protected by copyright. All rights reserved.

that was seen as a white spot in WT at ~6.2 Åï 1, was a peak at 2.5 Å in the FT spectrum, which corresponded to the interaction of Ru with the P atom in the vertical axis. This is in close agreement with the vertical axis Ruï P bond length of 2.4 Å detected by X-ray single crystal diffraction. Compared to the Ru-pincer, the relatively weaker signal in **PPRu** implied a weaker Ruï P coordination in the vertical axis.

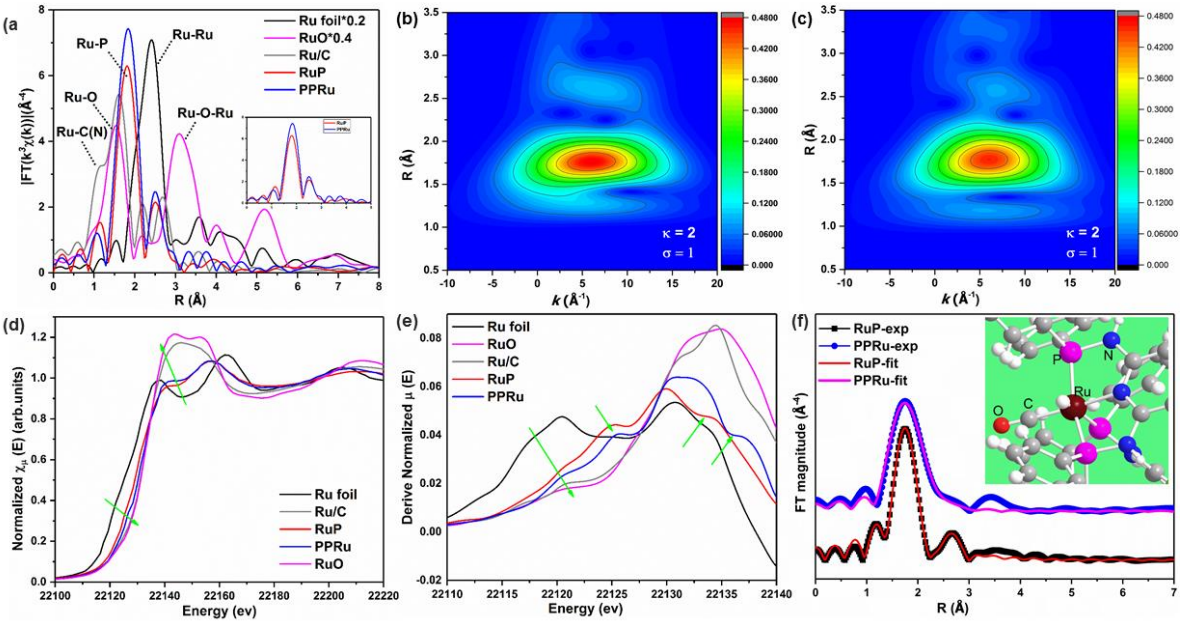

Figure 2. (a) Fourier transform magnitudes of the experimental Ru K-edge EXAFS spectra of the Ru-pincer precursor **RuP** and **PPRu** compared with reference materials. Wavelet transforms for the k2-weighted EXAFS signal of (b) **RuP** and (c) **PPRu**. The intensity maximum at 5.3 Åï 1 (R =1.8 Å) is associated with the horizontal axis Ruï P contributions and the second maximum at 6.3 Åï 1 (R =2.5 Å) is associated with the vertical axis Ruï P. (d) Normalized Ru K-edge XANES spectra. (e) First derivative curves. (f) Comparison between the Fourier transformed experimental Ru K-edge EXAFS.

XANES was also used to investigate the electronic structure of Ru in **PPRu**. The XANES spectra at the Ru K edge of the Ru-pincer precursor **RuP** and **PPRu** and those of the reference materials are shown in Figure 2d. It was observed that the overall profile of Ru/C was much closer to RuO rather than Ru metal foil, which suggested that Ru/C was heavily oxidized to RuO. As indicated by arrows, a clear trend of higher energy shift was observed from Ru foil to RuO, implying that their stable valence states increased from 0 to +2. This trend was further confirmed by the derivative XANES spectrum shown in Figure 2e. It was observed that the entire XANES spectrum of **PPRu** was identical to that of **RuP** and the overall profile was much closer to that of the RuO rather than metallic Ru, implying that the stable valences state was +2. The pre-edge peak, corresponding to a 1s-4p_z shakedown transition that is characteristic of a square-planar configuration,[21] showed weaker intensity for **PPRu** than **RuP**, suggesting a weaker coordination of the axial ligand. This observation was consistent with the XPS and WT analysis results. We then carried out XANES simulations of the architectural models. Since the single crystal X-ray crystallography data of the pincer precursor **RuP** was available,[12] the coordination numbers for Ruï N/C and Ruï P were fixed as 2 and 3 accordingly. The good agreement obtained between the experimental and calculated results for the Ru-pincer precursor

This article is protected by copyright. All rights reserved.

validated the reliability of our approach. Not surprisingly, the same model gave good fitting for **PPRu** with coordination numbers of 1.8 and 2.7 for Ruï N/C and Ruï P, respectively.

The porous properties of **PPRu** were analyzed by nitrogen sorption analysis (Figure S3a). Its Brunauerï Emmettï Teller (BET) surface area and total pore volume were found to be 810 m^2/g and 0.52 cm^3/g, respectively. **PPRu** exhibited a type I adsorption isotherm with a steep nitrogen gas uptake at low relative pressure ($P/P_0 < 0.01$), reflecting a microporous structure, a slight hysteresis loop indicating the presence of mesopores and a rise in nitrogen uptake at high relative pressure (P/P_0 = 0.9ï 1.0) was attributed to the presence of macropores.[1c] This was confirmed by the pore size distribution plot (Figure S3b) which showed that the pore sizes of **PPRu** were mainly distributed around 0.7 and 1.2 nm and some mesopores and macropores were also present. The bigger pore sizes can help improve mass transport and reduce diffusion limitations.[1c, 4c, 19b] Moreover, thermal gravimetric analysis (TGA) revealed that **PPRu** was thermally stable up to 260 °C (Figure S4).

With this single-atom dispersed heterogeneous ruthenium porous framework **PPRu** in hand, we explored its reactivity toward FA dehydrogenation. Not surprisingly, the pristine catalyst did not show any reactivity towards FA dehydrogenation under normal conditions with DMSO as solvent medium and triethylamine (TEA) as the base additive at 90 °C. This could be explained by our recent mechanistic studies of the homogeneous PN^3P-pincer ruthenium complexes, which showed that the dearomatized complex is the catalytically active species.[10] Accordingly, we treated **PPRu** with potassium *tert*-butoxide in DMSO for 24 h, and again applied it to FA dehydrogenation under the same conditions. The reaction proceeded smoothly, producing gases after a short induction period, indicating the catalyst had been successfully activated. The success in the activation of the catalyst manifested the advantage of our method, and this knowledge from the homogeneous catalyst could be directly transferred to the prepared heterogeneous catalyst.

Table 1. Catalyst performance over iterative use.[a]

Entry	Loading cycle	Conversion (%)	TOF ($h^{ï\,1}$)[b]
1	3	99	218
2	8	99	239
3	14	~100	248
4	17	~100	260
5	20	~100	266

[a]General conditions: T = 90 °C, FA (30 mmol, 1.2 mL), TEA (10 mmol, 1.5 mL), catalyst:FA = 1: 1500 (catalyst amount was equal to the amount of ruthenium pincer complex, which was calculated from the Ru content determined by ICP) in DMSO (5.0 mL). [b]Average TOF calculated after 3 h.

At the end of the first cycle, recharging the reaction flask with FA resulted in continued hydrogen production without any catalyst regeneration. In subsequent runs, the intermittent

This article is protected by copyright. All rights reserved.

addition of TEA was found to be important to maintain high TOF values. Interestingly, an increasing trend for TOF was observed over the course of 21 cycles in the **PPRu**/DMSO system (Table 1) with a TOF up to 266 h^{-1} in a single run (Table 1, Entry 5 and Figure S8). This may be ascribed to the swelling of the porous organic polymer, as seen in the SEM image of the recovered catalyst (Figure S11), which led to a more open structure and hence, better mass transport. FA was converted to gaseous products with nearly complete conversion (99%) within 24 h in all the recycles (Figure 3). Hot filtration and ICP-OES analysis indicated that the catalyst acted heterogeneously and the leaching of ruthenium species into the solution was negligible (<50 ppb), likely a result of the strong coordination of the PN^3P pincer ligand to Ru. Moreover, GC analysis showed that the produced gas consisted of H_2 and CO_2 without a trace of CO. This implied that the heterogeneous ruthenium catalyst had excellent selectivity for the dehydrogenation of FA into H_2 and CO_2 (Figure S10).

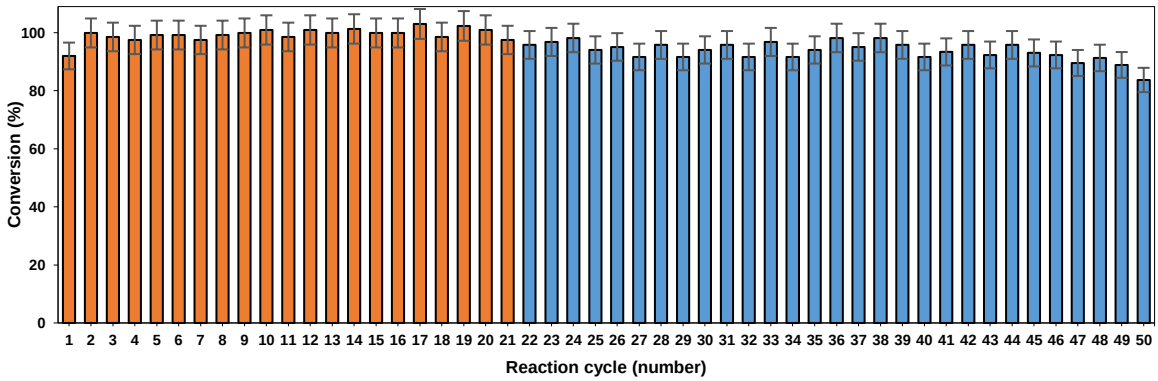

Figure 3. Recyclability test of the **PPRu** catalyst for the FA dehydrogenation reaction in DMSO (orange) and continuously in H_2O/DMSO (blue) after boiled in tap water.

Encouraged by these results, we further tested its performance toward FA dehydrogenation in aqueous medium. High stability towards water is crucial for applying the catalyst to real applications as commercially available FA always contains water. The **PPRu** catalyst recovered from the DMSO system after 21 cycles was further boiled in tap water for 24 hours in air and then subjected to DMSO/water (1:1, v/v) medium for FA dehydrogenation reaction. To the best of our knowledge, no pincer catalysts have ever been reported to be capable of tolerating such harsh conditions. Gratifyingly, in the aqueous medium, the **PPRu** catalyst continued to show a high conversion efficiency of ~97%, albeit slightly lower TOFs (170 h^{-1}) in the FA dehydrogenation reaction. The catalyst performance over iterative cycles was evaluated and is plotted in Figure 3. In a single, representative run, formic acid was converted to gaseous products with 97% conversion in 38 h (Figure S5) and afforded an average TOF of 172 h^{-1} (Table 2, Entry 2). It maintained a TOF of ~160 h^{-1} over 12 cycles without any significant decay in catalytic activity. After 50 cycles over a period of three months, a remarkable TON of 145,300 was obtained. In contrast, under the same reaction conditions, the homogeneous PN^3P-pincer ruthenium complex **RuP** gave a higher TOF of 1,806 h^{-1} and almost complete conversion (99%) in the first cycle. However, its catalytic activity dropped drastically in the subsequent cycles, suggesting its deactivation. In the second and third cycle, TOFs of 92 and 42 h^{-1} with conversion of 44% and 42% were obtained, respectively, and almost no gas formation could be observed in the fourth cycle, giving a total TON of 5,600. Such significantly enhanced stability of **PPRu** clearly indicates that besides the strong interactions of the N and P donor atoms with the Ru center in **RuP**, its knitting in the POPs by hyper-crosslinking with the spatial isolation

This article is protected by copyright. All rights reserved.

of the active sites was beneficial in preventing metal aggregation, migration and/or dissolution, thus promoting the long-term catalytic ability.

Table 2. Representative results of FA dehydrogenation using the heterogeneous **PPRu** complex.[a]

Entry	Solvent	Time (h)	Conversion (%)[b]	TOF (h^{-1})[c]
1	DMSO	24	99	266
2	DMSO/H_2O	38	94	172
3	H_2O	55	90	115
4	Toluene	21	97	208
5	DMF	54	92	138

[a]General conditions: T = 90 °C, FA (30 mmol, 1.2 mL), TEA (10 mmol, 1.5 mL), catalyst:FA = 1: 1500 (amount of the catalyst was equal to the amount of the ruthenium pincer complex, which was calculated from Ru content determined by ICP) in specified solvents. [b]Average conversion (based on three runs). [c]Average TOF calculated after 3 h.

Furthermore, the **PPRu** catalyst could also serve in other solvent medium such as DMF, toluene, and even H_2O itself with efficiency and reproducibility (Table 2). When the reaction was performed in pure H_2O, the catalyst gave the lowest TOF of 115 h^{-1} with 90% conversion, which could be attributed to the hydrophobic nature of the porous organic polymer. Such unmatched properties between the solvent and the support might compromise the activity by decreasing mass transfer inside the framework. Changing the solvent from H_2O to toluene resulted in a significant improvement in catalytic activity, giving a TOF value of 208 h^{-1} and 97% conversion. Very importantly, in all cases, the catalyst were stable and can be used repeatedly.

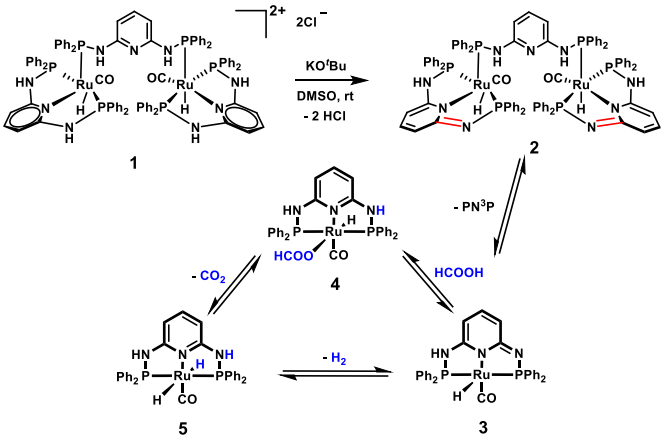

Scheme 2. Proposed mechanism for the Ph-PN^{3}P Ru-catalyzed FA dehydrogenation and CO_2 hydrogenation.

Based on our previous mechanistic studies of ^{t}Bu-PN^{3}P Ru-catalyzed homogeneous FA dehydrogenation[10] and the reverse reaction (hydrogenation of bicarbonate) using the Ru-pincer RuP,[12] we proposed a plausible mechanism, as shown in Scheme 2. The mechanism for the Ph-PN^{3}P Ru-catalyzed FA dehydrogenation involves the activation of **RuP** (**1**) by treatment with a strong base to form a dearomatized complex **2**, followed by the dissociation of the axial PN^{3}P ligand to give two coordinatively unsaturated 16-electron complexes **3**, which was

This article is protected by copyright. All rights reserved.

previously reported to be the catalytically active species.[10] The catalytic transformation involves three steps: protonation of the imine arm of the dearomatized pincer complex **3** to give the ruthenium formate intermediate **4**, decarboxylation of **4** to generate the dihydride species **5** with the liberation of CO_2, and the final elimination of H_2 that regenerates the catalyst. Accordingly, the lower TOF with **PPRu** as compared to the homogeneous PN^3P-pincer ruthenium complex in the first reaction cycle could presumably be a result of the slow dissociation of a PN^3P ligand from the bimetallic ruthenium complex in the solid state to give the catalytically active species. Nevertheless, the active species **3** covalently bonded with the framework and as it was spatially isolated, did not aggregate. As a result, **PPRu** exhibited the high reactivity and selectivity advantages of a homogeneous catalyst with enhanced catalyst stability and reusability characteristic of heterogeneous catalysis.

Conclusions

In summary, a new porous heterogeneous ruthenium catalyst (**PPRu**) with single-atomic sites was prepared by directly knitting a Ph-PN^3P-pincer ruthenium complex into a porous polymer network. The catalyst was then utilized for the conversion of FA to H_2. It was found that **PPRu** is a robust, water stable, reusable catalyst for FA dehydrogenation that demonstrates excellent selectivity and catalytic activity (TOF and TON up to 266 h^{-1} and 145,300, respectively). *The simple one-step knitting method described in this study offers new opportunities for the development of novel heterogeneous catalysts with significantly improved reactivity and durability.* Further studies on the catalytic applications of **PPRu** and the synthesis of other heterogeneous catalysts with single-atomic sites using this method are currently ongoing.

Supporting Information

Supporting Information is available from the Wiley Online Library or from the author.

Acknowledgements

We gratefully acknowledge the financial support from King Abdullah University of Science and Technology; Competitive Research Grant (URF/1/1378) and Baseline Funding, and from Chinese NSFC (51672309) and the Fundamental Research Funds for the Central Universities (18CX07009A).

Received: ((will be filled in by the editorial staff))
Revised: ((will be filled in by the editorial staff))
Published online: ((will be filled in by the editorial staff))

[1] a) C. McGlade, P. Ekins, *Nature*, **2015**, *517*, 187; b) E. I. Administration, G. P. Office, *International Energy Outlook 2016: With Projections to 2040*, Government Printing Office, 2016; c) X. Wang, Y. Liu, X. Ma, S. K. Das, M. Ostwal, I. Gadwal, K. Yao, X. Dong, Y. Han, I. Pinnau, *Adv. Mater.*, **2017**, *29*, 1605826.
[2] a) J. A. Turner, *Science*, **2004**, *305*, 972; b) S. Chu, A. Majumdar, *Nature*, **2012**, *488*, 294.
[3] a) P. P. Edwards, V. L. Kuznetsov, W. I. David, N. P. Brandon, *Energ Policy*, **2008**, *36*, 4356; b) S. Dutta, *J Ind Eng Chem*, **2014**, *20*, 1148.

This article is protected by copyright. All rights reserved.

[4] a) M. Felderhoff, C. Weidenthaler, R. von Helmolt, U. Eberle, *PCCP*, **2007**, *9*, 2643; b) N. Armaroli, V. Balzani, *ChemSusChem*, **2011**, *4*, 21; c) X. Wang, L. Xie, K.-W. Huang, Z. Lai, *Chem. Commun.*, **2015**, *51*, 7610.
[5] J. r. Eppinger, K.-W. Huang, *ACS Energy Letters*, **2016**, *2*, 188.
[6] a) M. Yadav, Q. Xu, *Energy Environ. Sci.*, **2012**, *5*, 9698; b) W.-H. Wang, Y. Himeda, J. T. Muckerman, G. F. Manbeck, E. Fujita, *Chem. Rev.*, **2015**, *115*, 12936; c) D. Mellmann, P. Sponholz, H. Junge, M. Beller, *Chem. Soc. Rev.*, **2016**, *45*, 3954; d) K. Sordakis, C. Tang, L. K. Vogt, H. Junge, P. J. Dyson, M. Beller, G. Laurenczy, *Chem. Rev.*, **2017**, *118*, 372.
[7] M. C. Orilall, F. Matsumoto, Q. Zhou, H. Sai, H. c. D. Abru¶a, F. J. DiSalvo, U. Wiesner, *J. Am. Chem. Soc.*, **2009**, *131*, 9389.
[8] a) C. Fellay, P. J. Dyson, G. Laurenczy, *Angew. Chem. Int. Ed.*, **2008**, *47*, 3966; b) A. Boddien, D. Mellmann, F. Gärtner, R. Jackstell, H. Junge, P. J. Dyson, G. Laurenczy, R. Ludwig, M. Beller, *Science*, **2011**, *333*, 1733; c) J. F. Hull, Y. Himeda, W.-H. Wang, B. Hashiguchi, R. Periana, D. J. Szalda, J. T. Muckerman, E. Fujita, *Nat. Chem.*, **2012**, *4*, 383; d) J. H. Barnard, C. Wang, N. G. Berry, J. Xiao, *Chem. Sci.*, **2013**, *4*, 1234; e) T. Myers, L. Berben, *Chem. Sci.*, **2014**, *5*, 2771; f) J. J. A. Celaje, Z. Lu, E. A. Kedzie, N. J. Terrile, J. N. Lo, T. J. Williams, *Nat. Commun.*, **2016**, *7*, 11308. g)
[9] a) K. Tedsree, T. Li, S. Jones, C. W. A. Chan, K. M. K. Yu, P. A. Bagot, E. A. Marquis, G. D. Smith, S. C. E. Tsang, *Nat Nanotechnol*, **2011**, *6*, 302; b) Q.-L. Zhu, N. Tsumori, Q. Xu, *J. Am. Chem. Soc.*, **2015**, *137*, 11743; c) Q. Liu, X. Yang, Y. Huang, S. Xu, X. Su, X. Pan, J. Xu, A. Wang, C. Liang, X. Wang, *Energy Environ. Sci.*, **2015**, *8*, 3204; d) C. Tang, A. E. Surkus, F. Chen, M. M. Pohl, G. Agostini, M. Schneider, H. Junge, M. Beller, *Angew. Chem. Int. Ed.*, **2017**, *56*, 16616.
[10] Y. Pan, C. L. Pan, Y. Zhang, H. Li, S. Min, X. Guo, B. Zheng, H. Chen, A. Anders, Z. Lai, J. Zheng, K.-W. Huang, *Chemistry–An Asian Journal*, **2016**, *11*, 1357.
[11] a) H. Li, B. Zheng, K.-W. Huang, *Coord. Chem. Rev.* **2015**, *293-294*, 116; b) C. Gunanathan, D. Milstein, *Chem. Rev.*, **2014**, *114*, 12024.
[12] C. Guan, Y. Pan, E. Ang, J. Hu, C. Yao, M.-H. Huang, H. Li, Z. Lai, K.-W. Huang, *Green Chem*, **2018**, DOI: 10.1039/c8gc02186d.
[13] a) Z. Wang, G. Chen, K. Ding, *Chem. Rev.*, **2008**, *109*, 322; b) P. Barbaro, F. Liguori, *Heterogenized homogeneous catalysts for fine chemicals production: materials and processes*, Vol. 33, Springer Science & Business Media, 2010.
[14] a) N. E. Leadbeater, M. Marco, *Chem. Rev.*, **2002**, *102*, 3217; b) R. Zhong, A. C. Lindhorst, F. J. Groche, F. E. K¿hn, *Chem. Rev.*, **2017**, *117*, 1970; c) X. Wang, S. Min, S. K. Das, W. Fan, K.-W. Huang, Z. Lai, *J. Catal.*, **2017**, *355*, 101.
[15] a) S. A. Burgess, A. Kassie, S. A. Baranowski, K. J. Fritzsching, K. Schmidt-Rohr, C. M. Brown, C. R. Wade, *J. Am. Chem. Soc.*, **2016**, *138*, 1780; b) M. Rimoldi, A. Nakamura, N. A. Vermeulen, J. J. Henkelis, A. K. Blackburn, J. T. Hupp, J. F. Stoddart, O. K. Farha, *Chem. Sci.*, **2016**, *7*, 4980.
[16] a) D. Wu, F. Xu, B. Sun, R. Fu, H. He, K. Matyjaszewski, *Chem. Rev.*, **2012**, *112*, 3959; b) Y. Zhang, S. N. Riduan, *Chem. Soc. Rev.*, **2012**, *41*, 2083; c) L. Tan, B. Tan, *Chem. Soc. Rev.*, **2017**, *46*, 3322.
[17] a) P. Kaur, J. T. Hupp, S. T. Nguyen, *Acs Catal.*, **2011**, *1*, 819; b) Q. Sun, Z. Dai, X. Meng, L. Wang, F.-S. Xiao, *Acs Catal.*, **2015**, *5*, 4556.
[18] a) S. Xu, Y. Luo, B. Tan, *Macromol Rapid Comm*, **2013**, *34*, 471; b) N. Fontanals, R. Marcé, F. Borrull, P. Cormack, *Polym Chem-Uk*, **2015**, *6*, 7231.

This article is protected by copyright. All rights reserved.

[19] a) B. Li, R. Gong, W. Wang, X. Huang, W. Zhang, H. Li, C. Hu, B. Tan, *Macromolecules*, **2011**, *44*, 2410; b) B. Li, Z. Guan, W. Wang, X. Yang, J. Hu, B. Tan, T. Li, *Adv. Mater.*, **2012**, *24*, 3390.
[20] M. Textor, L. Ruiz, R. Hofer, A. Rossi, K. Feldman, G. Hähner, N. D. Spencer, *Langmuir*, **2000**, *16*, 3257.
[21] C. Zhang, J. Sha, H. Fei, M. Liu, S. Yazdi, J. Zhang, Q. Zhong, X. Zou, N. Zhao, H. Yu, *ACS nano*, **2017**, *11*, 6930.

This article is protected by copyright. All rights reserved.